KSCE Journal of Civil Engineering (2024) 28(9):3591-3600
DOI 10.1007/s12205-024-0921-y

pISSN 1226-7988, eISSN 1976-3808
www.springer.com/12205

Environmental Engineering

Removal of Cs-137 from Real Liquid Radioactive Wastes Using Pumice in Fixed-Bed Column

Mezher Abed Gatea[a], **Ghufran Farooq Jumaah**[b], **Riyad Hassan Al anbari**[b], **and Qusay F. Alsalhy**[c]

[a]*Iraqi Decommissioning Directorate, Ministry of Science and Technology, Baghdad 10001, Iraq*
[b]*Dept. of Civil Engineering, University of Technology, Baghdad 10001, Iraq*
[c]*Dept. of Chemical Engineering, University of Technology, Baghdad 10001, Iraq*

ARTICLE HISTORY

Received 9 May 2023
Revised 24 January 2024
Accepted 26 March 2024
Published Online 31 May 2024

KEYWORDS

Pumice-fixed-bed
Radioactive liquids
Adsorption
Thomas and Clark models

ABSTRACT

Decontamination of the radiological pollutants takes a flagship role in the environmental restoration. It improves safety and minimizes the cost of the advanced activities. Therefore, this study was conducted to investigate the performance of pumice via a single-stage-fixed-bed column system to remove Cs-137 radionuclides from real liquid radioactive wastes (LRWs) and investigate the operation conditions affecting breakthrough occurrence. The pumice was pure, identified by a Fourier-transform infrared spectroscopy (FTIR), a scanning electron microscopy (SEM), a X-ray fluorescence spectrometry (XRF), and a X-ray diffraction (XRD) investigations. LRWs samples were radiologically characterized before and after decontamination by the gamma spectroscopy system with a high purity germanium (HPGe) detector. It is innovative and non-destructive test method. Results revealed that LRWs were contained a considerable concentrations of Cs-137 radioisotope. The maximum adsorption capacity was 106.47 kBq/g, which yielded at a bed depth of 0.2 cm, an influent discharge of 4 mL/min, a Cs-137 concentration of 19013.33 Bq/L, and a temperature of 20°C. The Thomas and the Clark models were appropriate for representing the data obtained from the experiments, because of their strong correlation factors 0.95 and 0.97, respectively. Results indicated that the adsorbed Cs-137 radionuclides increased with decreasing influent discharge and increasing radionuclides concentration. Based on the suitable models' nature, the Cs-137 adsorption process was impulsive, happened on monolayer and heterogeneous surfaces, and was controlled by chemical interactions onto active pumice sites.

1. Introduction

The radioactive waste is considered a significant part of the hazardous waste. It can be generated as solid, liquid or gas from many practices such as mining, radiotherapy, nuclear studies, electricity generation, and nuclear weapons. As a part of radioactive waste, liquid Radioactive Wastes (LRWs) comprise different radionuclides with Alpha, Beta/Gamma emitters. They have several adverse effects on organisms, such as increased body temperature (Boratyński et al., 2021), deposits in soft tissues and cells, irritating and ionizing the atoms, causing damage to chemical bonds, and even biological deterioration (Obrador et al., 2022). In addition, they affect many aquatic life species by accumulating in a muscle mass (Pereira et al., 2019). These effects can be created directly or indirectly through free radicals, which can easily damage the chemical bonds and alter DNA genetic mutation (Juan et al., 2021).

Generally, cesium is the main nuclide of concern in aqueous media (Karabayir et al., 2021). It is a soft, malleable, silvery-white element with the molecular symbol Cs. It readily combines with chlorides to create a powder that is crystalline. It melts at ambient temperature. Cesium-137, or Cs-137, is the most common radioactive form of the element. It is generated from nuclear fission. It releases high-energy beta particles that damage tissues by releasing energy when Cs-137 molecules break apart in cells. It also emits medium-energy gamma rays. Furthermore, internal

CORRESPONDENCE Mezher Abed Gatea ✉ bce.21.12@grad.uotechnology.edu.iq; mizher.abed@gmail.com Iraqi ☐ Decommissioning Directorate, Ministry of Science and Technology, Baghdad 10001, Iraq

exposure via the ingestion or inhalation of Cs-137 radionuclides can cause the released radioactivity to be mobile in the soft tissues, especially muscle tissue, exposing those tissues to beta particles and gamma radiation and increasing the risk of cancer (Metwally et al., 2017). Therefore, decontaminating Cs-137 radionuclides from LRWs is a crucial stage in radiation protection. It improves safety and minimizes the cost of the advanced activities (Park et al., 2017). It can be treated by precipitation (Osmanlioglu, 2018), resins (Tokar et al., 2022), reverse osmosis (Arnal et al., 2003), zeolite-membrane group (Abbas et al., 2022), electrochemical (Chen et al., 2020), solvent extraction (Xu et al., 2012), and adsorption process (Gatea et al., 2023).

The adsorption process is widely applied in water and wastewater treatment due to its efficiency and uncomplicated nature. It depends on both the adsorbate and adsorbent's chemical and physical nature. It is used to remove a broad range of pollutants like emerging pollutants (Al Ezzi and Ma, 2018), heavy metals (Chai et al., 2021), dyes (Nasar and Mashkoor, 2019), and radionuclides (Karabayir et al., 2019) through different adsorbents such as activated carbon, enhanced bio-char (Zhou et al., 2020), Nanoparticles adsorbents (Li et al., 2021), hierarchical adsorbents (Tuaimah et al., 2020), and others. One of the promising green materials adsorbents is the pumice. It is a high-porosity volcanic formation. It forms from lava with high water content, water vapour, and gases released from a volcano's impact. Natural and modified pumice was utilized in treatments of water and wastewater, such as support substances, filtration, adsorption, or to remove organic impurities like phenol and inorganic substances like heavy metals (Ratnawati et al., 2020).

Iraq has a problem with numerous facilities containing radioactive waste. Most of them were in the Al-Tuwaitha zone, southeast of Baghdad. These came from reactors, radio-chemical, and radio-medical operations. These operations have stopped since 1991, and the majority have been severely destroyed. One of the waste categories to be concerned about is the legacy LRWs. LRWs should be decontaminated in accordance with the ALARA concept and the allowable limits for the safe discharge to the surrounding environment to protect human health and the environment. In addition, the performance of natural pumice (without modification) in a fixed-bed column to adsorb Cs-137 radionuclides from real LRWs has not yet been verified in the literature. Therefore, this study was conducted to investigate the performance of the pumice via a single-stage-fixed-bed column system to remove Cs-137 radionuclides from real LRWs, taken from the Al-tuwaitha nuclear site and investigate the operation conditions affecting breakthrough occurrence.

2. Materials and Method

2.1 Preparation and Characterization of Pumice

The main material is pumice. It was purchased from a local scientific bureau for import to Iraq. It was ground as powdered using RETSCH grinder type (BB 50). The milled pumice was cleaned with ordinary water multiple times and double-cleaned with distilled water to remove pollutants. After that, it was dried and sieved by a series of sieves. So, the granular pumice, which passed through a sieve of 63 μm, was collected and implemented as an adsorbent material (Rajib and Oguchi, 2017).

X-ray diffraction (XRD), X-ray fluorescence spectrometry (XRF), scanning electron microscopy (SEM), and Fourier-transform infrared spectroscopy (FTIR) analyses were implemented to characterize the surface morphology, structure and chemical composition of pumice. An Ultima IV X-ray did the XRD test diffract meter (RIGAKU) instrument. The X-ray fluorescence spectrometer with wavelength dispersion PW 2400 Philips was utilized for XRF analysis. A computerized scanning electron microscopy (S-3000, Hitachi) was worked for the scanning electron microscope (SEM) spectrometry integrated analysis system. As well as a Fourier-transform infrared spectroscopy (FTIR) was exploited to detect a spectrum of the infrared emissions of the pumice. It is from Shimadzu Europe company. Furthermore, a 10 g of pumice powder and 100 mL of distilled water were mixed slowly by a magnetic stirrer plate for an hour to determine the pH of the pumice (Ismail et al., 2014). Subsequently, filter paper was used to filter the pumice slurry and a pH meter of the Lovibond type (Senso Direct 150) was used to detect the pH of the filtered water.

2.2 Collection and Preparation of LRWs Samples

Two samples of LRWs, 15 and 25 mL, were taken from the Al-Tuwaitha's liquid waste tanks. The initial concentrations of C1 and C2 were prepared for each sample by adding one litter of distilled water (Agency, 2007). The initial pH was 5.

2.3 Description of Single-Stage-Fixed-Bed Column System

The study of radionuclide adsorption on the pumice material was implemented in a single-stage, fixed-bed column system at a temperature of 20ºC. Figs. 1(a) and 1(b) shows the extraction chromatography column used to perform tests. It consists of columns, a box, a pressure gauge, and a pump. The column was made from fiberglass. It enlarges at the upper end to has a diameter of 1.6 cm for a length of 1.7 cm, then its diameter shrinks to be 0.6 cm for a length of 8.4 from its lower end. It was connected at the upper end with a movable frustum cone funnel to contain and pass the contaminated liquid per the designed discharge. The box was 25 × 10 × 15 cm, made of fiberglass, has 12 injection columns, each with a plastic tap at the upper end to control the liquid flow rate and a container at the bottom to collect the treated liquid. The pump (04W1120) had a maximum discharge volume of 28 L/min and operated at 220 V/50 Hz. A pressure gauge of 0 − 30 inch Hg was connected between the box and the vacuum pump to regulate the pressure to achieve the proper liquid discharge.

2.4 Fixed-Bed Column Experiments

A single-stage-fixed-bed column system was used to study the relationship between the bed thickness of the pumice stone, the

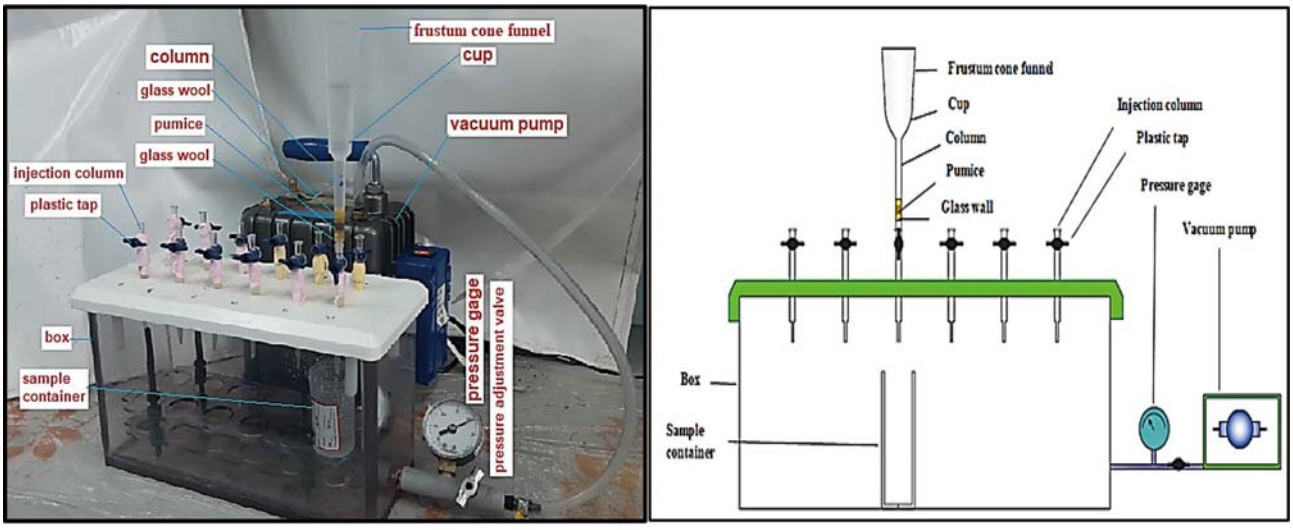

Fig. 1. Column Chromatography System: (a) Picture, (b) Graph

Cs-137 radionuclides concentration in the LRWs, and the influent discharge of this liquid. Two concentrations from the real LRWs were used. For each one, two fixed-bed thicknesses (H1 of 0.2 cm and H2 of 0.4 cm) were applied individually to examine two discharges of 4 and 6 mL/min. All the preceding parameters were investigated at different adsorption times of 5, 10, 20, 30, 60, 120, 180, and 240 minutes. The pH and the temperature of the LRWs were constant at 5 and 20°C, respectively.

A known value of the pumice was loaded carefully into the column as a fixed bed and sandwiched by a glass wool to maintain stability. The distilled water was vacuumed through the column before testing to prevent the possible forming of voids and channelling. Steadily, an amount of LRWs was loaded onto the column, the tap was opened, the vacuum pump was allowed to operate, and the pressure gauge was adjusted to produce the aimed discharge. The effluent sample was collected in a plastic container at the end of the column. Finally, the polluted pumice was disposed of in a double-layered nylon bag-lined shielded barrel (Gatea and Kadhum, 2019). To minimize volume, the barrel will be compacted using a compaction tool. After that, it will be buried in a repository beneath the earth.

2.5 Characterization of LRWs

A gamma radiation spectrometer system was utilized to characterize the LRWs before and after decontamination. It depends upon emissions of the energy-related gamma lines for each radionuclide. It was made by ORTEC company. It consists of three components. The first is a *Detector of High purity Germanium* (*HPGe*) type (GEM65P4-95), co-axial tool and pure germanium crystal. The detector diameter is 71.9 mm, and the length is 73.1 mm. A lead barrier of 10 cm surrounded the HPGe detector for radiation protection. The detector operates under extreme cold by liquid nitrogen. The second is a *Pre-amplifier*, model A257P. The third is *Analytics channels,* which involve 8000 units to document pulses through their depths.

A known activity concentration standard sources are used to continuously calibrate the system. To create a sample of 250 mL that was comparable to the standard container of the calibration source of the gamma spectrometer system, 10 mL of each sample of LRWs, both before and after decontamination, were taken, put in a standard container, and diluted with the distilled water. After that, the filled container spent an hour inside a gamma spectrometer. The results of the radionuclide type and concentration were shown in Bq/L units on the attached computer. The concentration of each sample was then modified in accordance with the dilution ratio (Gatea et al., 2024).

2.6 Column Data Analysis

The breakthrough and exhaustion (saturation) concentrations were described as the concentration of radionuclides in the effluent equal to 10% and 90% of the influent concentration, respectively (Abdolali et al., 2017). The curve and time (t_b) of breakthrough are the main features that conclude from the packed-bed column adsorption mechanism. The curve of the breakthrough is formed by variation of the ratio of effluent to influent radionuclide concentrations C_e/C_O as a function of adsorption time. Eqs. (1) and (2) express the saturation time and the breakthrough, respectively (Geleta et al., 2021).

$$t_e = \int_{t=0}^{t=t_{total}} \left(1 - \frac{C_e}{C_0}\right) dt, \tag{1}$$

$$t_b = \int_{t=0}^{t=t_b} \left(1 - \frac{C_e}{C_0}\right) dt, \tag{2}$$

where t_e = the saturation time (min), t_b = the breakthrough time (min).

The total amount of the adsorbed radionuclides in the fixed-

bed column for a specified feed concentration (C_e) and the initial discharge (Q) can be obtained from Eq. (3) (Han et al., 2009).

$$q_{total} = QA\int_{t=0}^{t=t} total\left(1-\frac{C_e}{C_0}\right)dt, \quad (3)$$

where Q = the discharge rate (mL/min), and A = the area under the breakthrough curve.

The adsorption capacity (q_e) of the column is the maximum quantity of the adsorbed Cs-137 radionuclides onto the pumice particles at equilibrium status. It is a key of adsorbent material (de Araujo et al., 2022). It is calculated as the ratio of the total quantity of the adsorbed radionuclides (q_{total}) to the amount of dry mass of the implemented pumice (m) as in Eq. (4).

$$q_e = \frac{q_{total}}{m} = \frac{C_0 Q t_e}{m} \quad (4)$$

The experimental adsorption capacity (q_b) or the quantity of the removed radionuclides at (t_b) can be estimated by Eq. (5).

$$q_b = \frac{C_0 Q t_b}{m} \quad (5)$$

Equations (6) and (7) were implemented to estimate the liquid volume at breakthrough (V_b) in (mL) units until the breakthrough time and the total volume of the effluent (V_e) in (mL) units until saturation time, respectively.

$$V_b = Qt_b \quad (6)$$

$$V_e = Qt_e \quad (7)$$

The mass transfer zone (MTZ) is the area of largest mas transfer rate. It is evolving with adsorption process in the fixed-bed column system (Qian et al., 2019). Eq. (8) (Futalan et al., 2020) introduces the MTZ calculation.

$$MTZ = H_T\frac{(t_e - t_b)}{t_e}, \quad (8)$$

where H_T = total bed height (cm), t_e = saturation time (min), t_b = breakthrough time (min).

2.7 Modelling of Breakthrough Curves

The three numerical models applied to represent the adsorption mechanism in the pumice fixed-bed column are presented below.

2.7.1 Thomas Model

The model is presented in Eq. (9) (Cruz-Olivares et al., 2013).

$$\frac{C_e}{C_0} = \frac{1}{1+exp\left[K_T q_0 \frac{m}{Q} - K_T C_0 t\right]}, \quad (9)$$

where K_T = Thomas rate constant (L/min Bq), C_0 = initial concentration (Bq/L), C_e = effluent concentration of the Cs-137 radionuclides at the time t (Bq/L), Q = discharge (mL/min), q_o = equilibrium adsorbate uptake (Bq/g) and m = weight of pumice in a fixed-bed (g).

2.7.2 Adams-Bohart Model

The form of the Adams–Bohart model is Eq. (10) (Cruz-Olivares et al., 2013).

$$\frac{C_e}{C_0} = \frac{1}{1+exp\left[K_{AB}N_o\frac{Z}{v} - K_{AB}C_0 t\right]}, \quad (10)$$

where K_{AB} = kinetic constant (L/Bq·min), v = linear discharge (mL/min), Z = column bed depth (cm), N_O = saturation concentration (Bq/L), and t = time ranges (min) from the start to breakthrough. The linear flow rate (superficial velocity) was calculated by Eq. (11).

$$v = \frac{Q}{A}, \quad (11)$$

where A = cross-sectional area of the fixed-bed (cm^2) and Q = discharge rate (mL/min).

2.7.3 Clark Model

Equation (12) represents the Clark model (Altufaily et al., 2019).

$$\frac{C_e}{C_0} = \left[\frac{1}{1+Ae^{-rt}}\right]^{1/(n-1)}, \quad (12)$$

where n = Freundlich factor; A and r are Clark model constants that represent the slope and intercept of a plot between $\left[\left(\frac{C_0}{C_e}\right)^{n-1}-1\right]$ and time.

2.8 Uncertainty of Measurements

The HPGe system is a tool used to measure radionuclides activities in the LRWs and the uncertainty of the measurement (Raut et al., 2020). The working principle of this system is based on the generated electrical signals from gamma emissions that result from radioactive decay. This conversion is time-varying and dependent on various elements, including the transformed medium, calibration of the system, effectiveness of detection, and the laboratory conditions. As a result, the repeatedly characterization of LRWs using the HPGe system produces slightly different measurements. When presented graphically, each data point has an associated uncertainty value that represents the measurement procedure' inherent standard deviation. The uncertainty measurement is constantly kept below 5%, which is regarded as a reasonable and believable standard (Tomkins, 2014; Ravindra et al., 2023).

3. Results and Discussion

3.1 Characterization of Pumice

In the XRD analysis of the pumice composition shown in Fig. 2(a), there were high peaks of (2 Theta) in the curve at 23.4, 26.7, 31.1, 33.4, 36, 38.2, 43.3, 45.5, 50.1, 52.4, 57.2, 61.8, 64.7, and 71.6°. The major minerals of the pumice composition through XRD results were fassaite mineral ($Al_{0.433}Ca_{0.968}Fe_{0.22}Mg_{0.578}Si_{1.728}Ti_{0.059}O_6$) and diopside mineral ($CaMgSi_2O_6$) at 48% and 52%, respectively.

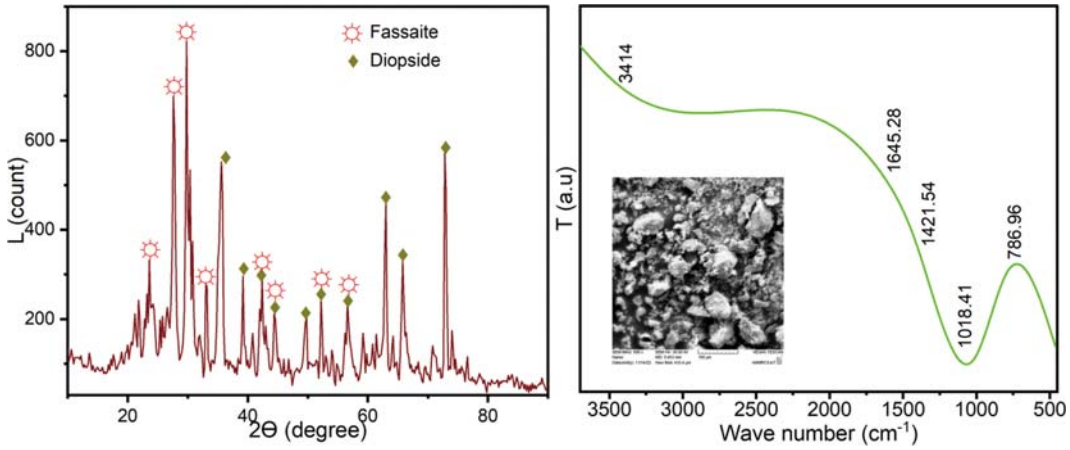

Fig. 2. Identification of Pumice: (a) XRD Analysis, (b) FTIR Spectrum and SEM Tests

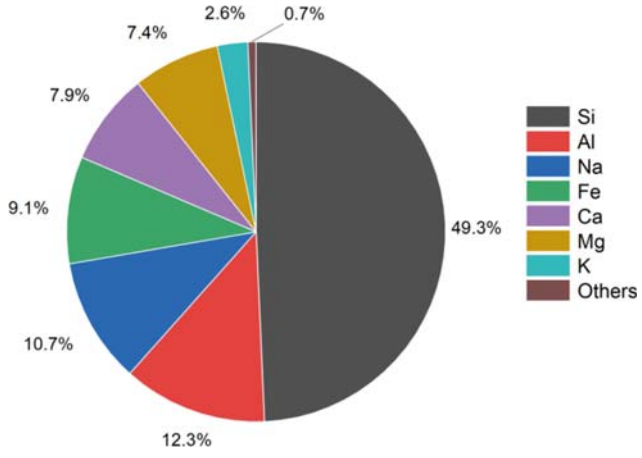

Fig. 3. The Dominant Elements in Pumice

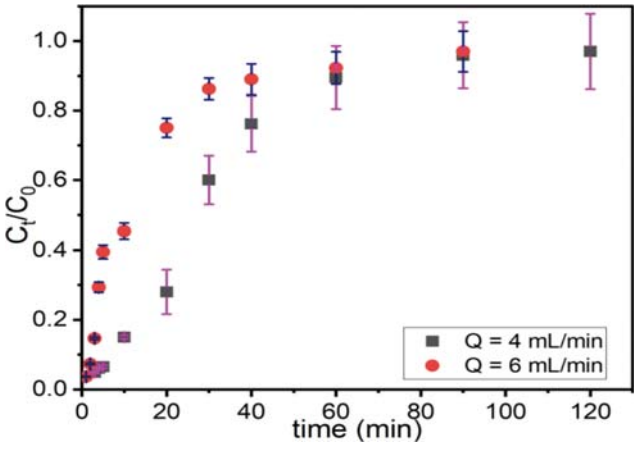

Fig. 4. Effect of Influent Discharge on Cs-137 Radionuclides Adsorption Onto Pumice ((bed depth = 0.2 cm, C= 19013.33 Bq/L, pH = 5, temperature = 20°C))

The weights of elements in the XRF analysis presented in Fig. 3 corroborate the XRD findings, revealing that the main elements in pumice were Si, Al, Fe, Mg, Na, and K. Therefore, the pumice was natural (Ersoy et al., 2010). Fig. 2(b) presents the FTIR domain of the pumice powder. The distinctive peaks of wave number were 786.96, 1018.41, 1421.54, 1645.28, 3414, and 3739.97 cm^{-1}. The two wavelength 786.96 and 1018.41 cm^{-1} are the fluctuations of the bend and stretch of the Si-O correlation, respectively. The wavelength below 1450 cm^{-1} is the natural structure of the pumice. The peaks of 1645.28 and 3739.97 cm^{-1} are the bend and stretch correlations of the H-O-H. In addition, Fig. 2(b) shows the SEM photo of the pumice particles. It shows particles of different sizes, rough surfaces, and sharp edges due to high cavities.

3.2 Characterization of LRWs

LRWs are radiologically characterized by a gamma spectroscopy with a HPGe detector. The initial concentrations were 4623 and 19013.33 Bq/L for C1 and C2, respectively. The results revealed that LRWs were contained a considerable concentrations of Cs-137 radioisotope comparing with the level of 11 Bq/L for human consumption (Nuccetelli et al., 2012).

3.3 Factors Affecting Fixed-Bed Adsorption Performance

The factors of discharge, bed depth, and radionuclides concentration were studied to evaluate a single-stage pumice-fixed-bed column performance.

3.3.1 Influent Discharge

The breakthrough curves for two down flow discharges (4 and 6 mL/min) are illustrated in Fig. 4, with a bed depth of 0.2 cm, a pH of LRWs of 5, an initial Cs-137 concentration of 19013.33 Bq/L, and a temperature of 20°C. An increase in the discharge led to steeper breakthrough curves. The slow motion of 4 mL/min may have created a suitable contact time for relocating (Cardona et al., 2023) the radionuclides onto the pumice by allowing Cs-137 radionuclides to permeate in the pumice cavities and occupy additional active sites of the alkali metals like K^+ and Na^+ within the pumice. In addition, the diffusion resistance of the external contact layer decreased, resulting in a well distribution of LRWs in the fixed-bed column and ultimately maximizing the diffusivity of Cs-137 radionuclides among the pumice particles (Daffalla et

Table 1. Operating Conditions of the Pumice Fixed-Bed Column

Z cm	C_0 Bq/L	Q_0 mL/min	t_b min	t_e min	V_b mL	V_e mL	MTZ cm	q_{total} kBq	q_e kBq/g	q_b kBq/g
0.2	4623	4	4	151	16	604	0.10	2.79	27.93	0.75
		6	2	35	12	210	0.20	0.98	9.77	0.55
0.4	4623	4	11	137	44	548	0.30	2.53	8.44	0.67
		6	5	80	30	480	0.40	2.21	7.39	0.46
0.2	19013.33	4	3	140	12	560	0.10	10.64	106.47	2.28
		6	1	67	6	402	0.20	7.7	77.00	1.14
0.4	19013.33	4	4	155	16	620	0.30	11.78	39.29	0.95
		6	2	46	12	276	0.40	5.24	17.49	0.76

al., 2022). Thus, a higher adsorption capacity was attained (i.e., 106.47 kBq/g). Therefore, the best pumice performance was with the lowest LRWs discharge.

Table 1 shows the breakthrough report. For Cs-137 concentration of 19013.33 Bq/L and a bed depth of the pumice of 0.2 cm, an increasing discharge from 4 to 6 mL/min lead to a reduction in the breakthrough time from 3 to 1 min, the saturation time decreased from 140 to 67 min, and decreased the volume of the treated LRWs from 560 to 402 mL. Consequently, the column's maximum adsorption capacity (q_e) and the adsorption capacity at breakthrough time (q_b) were decreased from 106.47 to 77 kBq/g and from 2.28 to 1.14 kBq/g, respectively, when the discharge increased from 4 to 6 mL/min. Likewise, in Table 1, when the Cs-137 concentration lowered to 4623 Bq/L in the moved LRWs through 0.2 cm bed depth in the two separate discharges of 4 and 6 mL/min, the values of breakthrough and exhaustion time were decreased from 4 to 2 min and from 151 to 35 min, respectively. The volume of the treated LRWs lowered from 604 to 210 mL with increasing discharge. In addition, q_{total}, q_e and q_b were reduced from 2.79 kBq, 27.93 kBq/g, and 0.75 kBq/g to 0.98 kBq, 9.77 kBq/g, and 0.55 kBq/g, respectively, with increasing discharge of LRWs from 4 to 6 mL/min. This is due to that the quantity of the adsorbed Cs-137 radionuclides through a unit bed of height MTZ is rapidly enlarged, speeding the saturation of bed and decreasing the residence time for Cs-137 radionuclides onto the pumice surface (Patel et al., 2022). The MTZ may enhanced via the increasing molecules in the growing adsorption layer (Hadi et al., 2011). In addition, the effect of the discharge variation was recorded for the overall breakthrough parameters in Table 1 when the layer depth increased to 0.4 cm for both concentrations of Cs-137 radionuclides. El-Kamash (2008) concluded from a study used zeolite in a fixed-bed column system to remove radionuclides from aqueous waste, the uptake of radionuclides decreased with increasing discharge rate and increased with increasing initial radionuclide concentrations and bed height.

3.3.2 Bed Depth

Figure 5 illustrates the adsorption behavior of the Cs-137 radionuclides onto pumice at two-bed depths with a concentration of 19013.33 Bq/L, a pH of 5, a temperature of 20°C, and a down flow discharge of 4 mL/min. The study tested two-bed depths of 0.2 and 0.4 cm, which formed from a 0.1 and 0.3 g dry weight of the pumice, respectively. Fig. 5 shows a noticeable increase in the breakthrough time and the saturation time with an increase in the bed depth from 0.2 to 0.4 cm. For the 0.2 cm bed depth, the breakthrough and the saturation time occurred at 3 min and 140 min, respectively. In contrast, the 0.4 cm bed depth occurred at 4 min and 155 min, respectively. This behavior was related to the larger specific surfaces, suitable adsorption time, and more active sites to bind Cs-137 radionuclides onto the pumice with increasing bed depth (Soto et al., 2017). An increase in the bed depth yielded an additional mass transfer zone that caused a more decline in the breakthrough curves. When the bed depth was increased, there was more mass transfer than axial diffusion. Other studies (Acheampong et al., 2013; Riazi et al., 2016; Zhang et al., 2019) have concluded that for better fixed-bed column sorption, beds with a higher amount of adsorbent would be more effective to provide additional active sites for sorption.

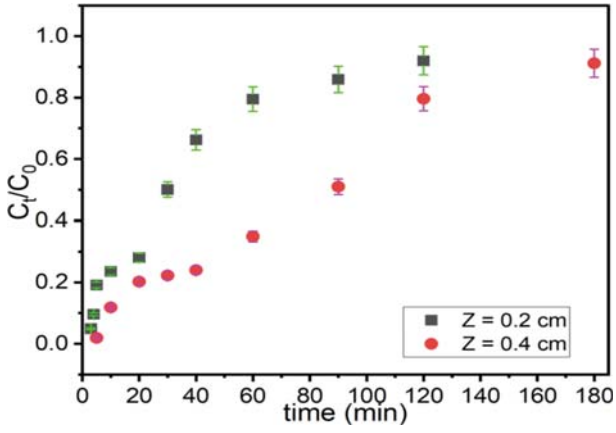

Fig. 5. Effect of Bed Depth on Cs-137 Radionuclides Sorption onto Pumice (Q = 4 mL/min, C= 19013.33 Bq/L, respectively, pH = 5, temperature = 20°C)

3.3.3 Concentration of Inlet Cs-137 Radionuclides

The effect of the change in concentration on the breakthrough curves is presented in Fig. 6, using a pH of LRWs of 5, a temperature of 20°C, a bed depth of 0.2 cm, and a down flow discharge rate of 4 mL/min. The breakthrough curves for Cs-137 radionuclides occurred due to alterations in the influent concentration in the column bed. Fig. 6 reveals that the style and the slope of

the breakthrough curves were remarkably different with an increase and decrease in the Cs-137 radionuclides concentration. Increasing the Cs-137 radionuclides concentration in the moving LRWs through the fixed-bed column produced a noticeable reduction of the treated LRWs volume to get the breakthrough point. The treated LRWs volume (Table 1) was changed from 604 mL at the lowest concentration of 4623 Bq/L to 560 mL at the highest concentration of 19013.33 Bq/L. The radionuclides with a higher concentration (19013.33 Bq/L) yielded shorter breakthrough and saturation times, which were 2 min and 140 min, respectively, than the lowest concentration (4,623 Bq/L), which were 3 min and 151 min, respectively. The early breakthrough and saturation time could have resulted from the higher amount of Cs-137 radionuclides in a higher concentration, which provided less mass transfer impedance (Patel, 2020). These findings demonstrated that the Cs-137 radionuclides' removal mode is significantly concentration-reliant. A lower impeding force for the radionuclide transfer and a greater concentration inclination were predicted at higher concentrations (Cardona et al., 2023). Moreover, the lowest concentration (4,623 Bq/L) had a smaller slope than the curve of the higher concentration (19013.33 Bq/L) in Fig. 6. It means less transformation of Cs-137 radionuclides between the contact layer of LRWs and the pumice surface. These outcomes assume that altering the initial adsorbate concentration as a kinetic force influenced the saturation rate and the breakthrough time (Chen et al., 2012). Therefore, the adsorption capacity increased from 27.93 to 106.47 kBq/g by increasing the inlet concentration of Cs-137 radionuclides in the LRWs from 4623 to 19013.33 Bq/L.

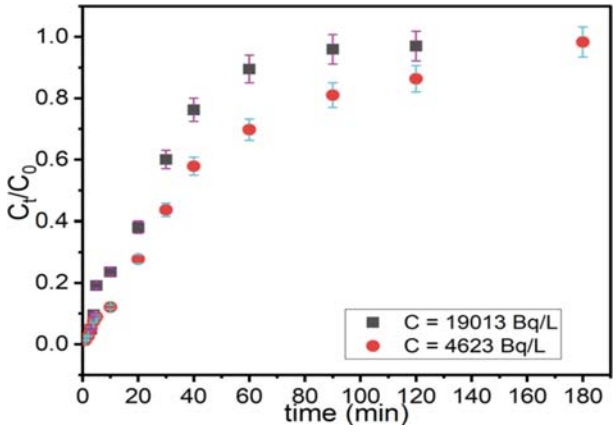

Fig. 6. Effect of Concentration of Cs-137 Radionuclides Sorption onto Pumice (pH = 5, bed depth = 0.2 cm, and at temperature = 20°C)

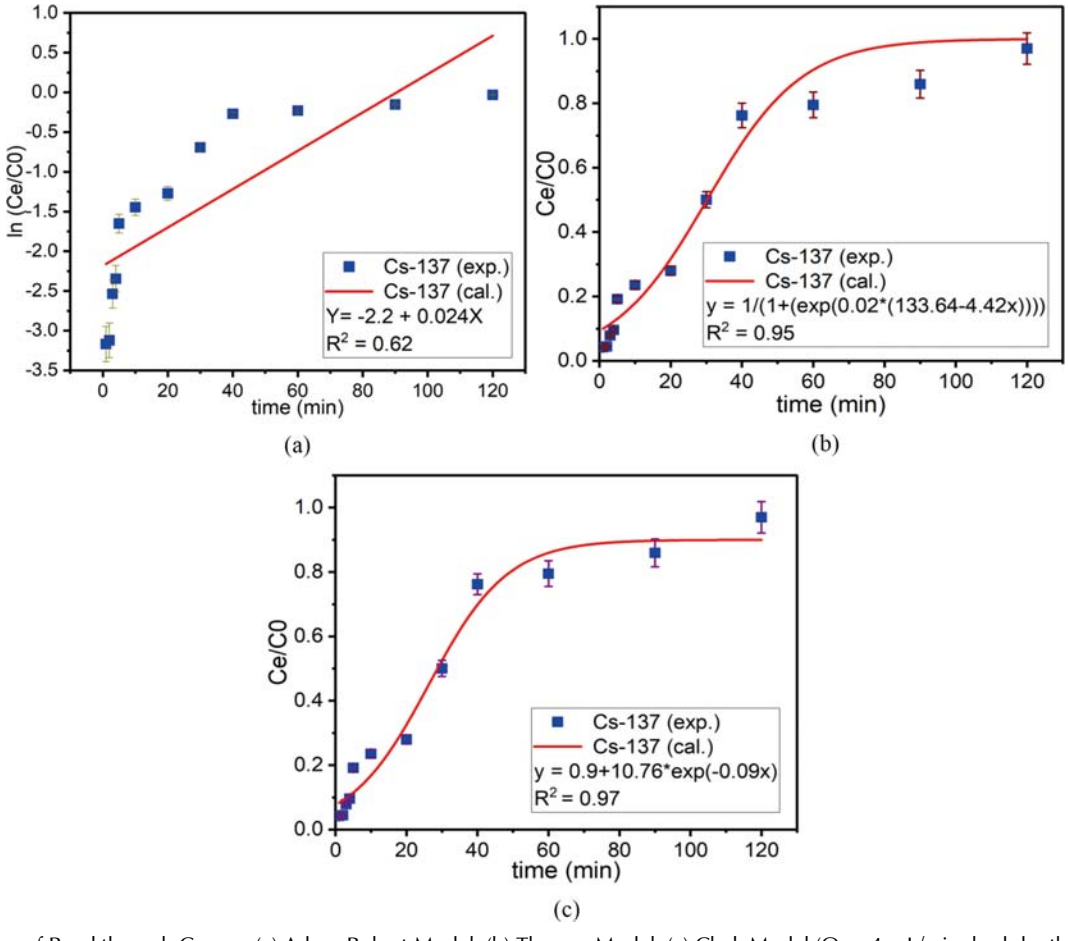

Fig. 7. Modeling of Breakthrough Curves: (a) Adam-Bohart Model, (b) Thomas Model, (c) Clark Model (Q = 4 mL/min, bed depth = 0.2 cm, pH = 5, temperature = 20°C, and C = 19013.33 Bq/L)

3.4 Modelling of Breakthrough Curves

The models of the Adams-Bohart, the Clark and the Thomas were applied to the experimental parameters of a fixed-bed system at operating conditions of a down flow discharge of 4 mL/min, a bed depth of 0.2 cm, a pH of 5, a temperature of 20ºC, and a Cs-137 concentration of 19013.33 Bq/L. The achieved results for the models were plotted and are illustrated in Fig. 7. It displays the correlation factors for the Adams–Bohart, the Thomas, and the Clark models, which were 0.62, 0.95, and 0.97, respectively. Therefore, both the Clark and the Thomas models are the optimal models to represent the obtained data. Based on the suitable models' nature and the simulation processes, the radionuclide adsorption process was impulsive, occurred on monolayer and heterogeneous surfaces, and was controlled by chemical interactions onto the active pumice sites (Chen et al., 2013).

4. Adsorption Mechanism

The adsorption mechanism can be interpreted through knowing the behaviour of the related statistical models with the experimental results. For the Clark and the Thomas models, the regression factors (R^2) were 0.97 and 0.95, respectively. Hence, Both the Clark and the Thomas models are supported by the data obtained from the down flow fixed-bed column adsorption of Cs-137 radionuclides onto the pumice. The Thomas model considers that the interaction process in the fixed-bed column yields the Langmuir adsorption mechanism (Cruz-Olivares et al., 2013) while, Clark's model adopted the idea that group exchange in adsorption follows the Freundlich isotherm (Altufaily et al., 2019). Therefore, the adsorption process occurred on mono-layer and heterogeneous surface. On the other hand, Fig. 8 shows the more affected elements of pumice, which analyzed by XRF analysis before and after adsorption of Cs-137 radionuclides. There is an apparent decline in the weight of K^+ and Na^+ cations after adsorption compared with their weights in the used pumice. The decline in K^+ and Na^+ weights belongs to the ion exchange process between Cs-137 radionuclides and the mentioned cations (Abbas et al., 2022; Gatea et al., 2024).

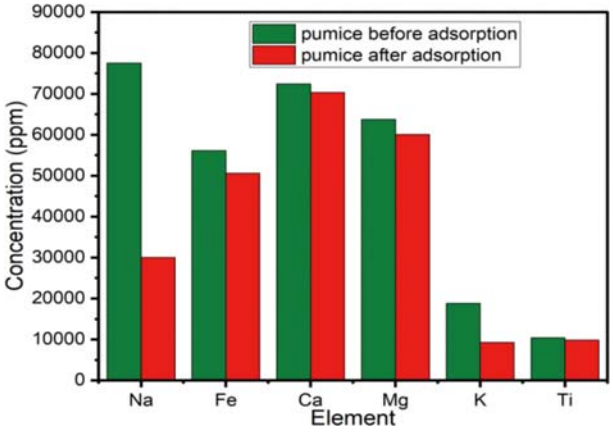

Fig. 8. The XRF Analysis Shows the Main Interchanged Elements of Pumice with Cs-137 Radionuclides (0.2 cm bed depth, 4 mL/min Influent Discharge, and Cs-137 Concentration of 19013.33 Bq/L at 20ºC)

5. Conclusions

The pumice in a down flow single-stage fixed-bed column system showed a significant efficiency in eliminating Cs-137 radionuclides from real LRWs. Its characteristics elucidated that it is a natural material. LRWs were characterized by a gamma spectrometry system and revealed that the liquid was contaminated with Cs-137 radionuclides. The discharge, the bed depth and the initial concentrations of Cs-137 radionuclides were used to evaluate the pumice-fixed-bed column efficiency. The results proved that the adsorption performance was inversely proportional to the discharge and directly proportional to the Cs-137 radionuclides concentration in the LRWs. The Adam-Bohart, the Thomas and the Clark models were used as numerical models to represent the dynamic mechanism of the adsorption process. The models were applied at a 4 mL/min down flow discharge, a 0.2 cm bed depth, a pH of 5, a temperature of 20ºC, and a Cs-137 concentration of 19013.33 Bq/L. The correlation factors for the preceding models were 0.62, 0.95, and 0.97, respectively, indicating that the Clark and the Thomas models were more significant in explaining the obtained experimental data than the Adam-Bohart model. Based on the suitable models' nature and the simulation process, the radionuclides' adsorption process was impulsive, happened on monolayer and heterogeneous surfaces, and was controlled by chemical interactions onto active pumice sites.

Acknowledgments

Thanks to the University of Technology for providing vital information and contemporary sources, and the authors acknowledge the Iraqi Atomic Energy Committee (IAEC) for their assistance in sampling and characterizing the (LRWs).

ORCID

Mezher Abed Gatea https://orcid.org/0000-0003-1504-0649
Ghufran Farooq Jumaah https://orcid.org/0000-0003-1613-2959
Qusay F. Alsalhy https://orcid.org/0000-0002-0495-1300

References

Abbas TK, Rashid KT, Alsalhy QF (2022) NaY zeolite-polyethersulfone-modified membranes for the removal of cesium-137 from liquid radioactive waste. *Chemical Engineering Research and Design* 179:535-548, DOI: 10.1016/j.cherd.2022.02.001

Abdolali A, Ngo HH, Guo W, Zhou JL, Zhang J, Liang S, Chang SW, Nguyen DD, Liu Y (2017) Application of a breakthrough biosorbent for removing heavy metals from synthetic and real wastewaters in a lab-scale continuous fixed-bed column. *Bioresource Technology* 229:78-87, DOI: 10.1016/j.biortech.2017.01.016

Acheampong MA, Pakshirajan K, Annachhatre AP, Lens PN (2013) Removal of Cu (II) by biosorption onto coconut shell in fixed-bed

column systems. *Journal of Industrial and Engineering Chemistry* 19:841-848, DOI: 10.1016/j.jiec.2012.10.029

Agency IAE (2007) Strategy and methodology for radioactive waste characterization. IAEA Vienna

Al Ezzi A, Ma H (2018) Equilibrium adsorption isotherm mechanism of water vapor on zeolites 3A, 4A, X, and Y. ASME International Mechanical Engineering Congress and Exposition, 2017. American Society of Mechanical Engineers, V006T08A059, DOI: 10.1115/IMECE2017-72601

Altufaily MAM, AL-Mansori NJ, AL-Qaraghulee AFM (2019) Mathematical modeling of fixed-bed columns for the adsorption of methylene blue on to fired clay pot. *International Journal of ChemTech Research* 12:70-80, DOI: 10.20902/IJCTR.2019.120210

Arnal J, Sancho M, Verdú G, Campayo J, Villaescusa J (2003) Treatment of 137Cs liquid wastes by reverse osmosis Part I. Preliminary tests. *Desalination* 154:27-33, DOI: 10.1016/S0011-9164(03)00205-4

Boratyński Z, Mousseau TA, Møller AP (2021) Individual quality and phenology mediate the effect of radioactive contamination on body temperature in Chernobyl barn swallows. *Ecology and Evolution* 11:9039-9048, DOI: 10.1002/ece3.7742

Cardona Y, Korili SA, Gil A (2023) Use of response surface methodology to optimize triclosan adsorption on alumina pillared clays in a fixed-bed column for applications in solid-phase extraction. *Applied Clay Science* 235:106879, DOI: 10.1016/j.clay.2023.106879

Chai WS, Cheun JY, Kumar PS, Mubashir M, Majeed Z, Banat F, Ho S-H, Show PL (2021) A review on conventional and novel materials towards heavy metal adsorption in wastewater treatment application. *Journal of Cleaner Production* 296:126589, DOI: 10.1016/j.jclepro.2021.126589

Chen J, Cai Y, Clark M, Yu Y (2013) Equilibrium and kinetic studies of phosphate removal from solution onto a hydrothermally modified oyster shell material. *PLoS One* 8:e60243, DOI: 10.1371/journal.pone.0060243

Chen S, Hu J, Han S, Guo Y, Belzile N, Deng T (2020) A review on emerging composite materials for cesium adsorption and environmental remediation on the latest decade. *Separation and Purification Technology* 251:117340, DOI: 10.1016/j.seppur.2020.117340

Chen S, Yue Q, Gao B, Li Q, Xu X, Fu K (2012) Adsorption of hexavalent chromium from aqueous solution by modified corn stalk: A fixed-bed column study. *Bioresource Technology* 113:114-120, DOI: 10.1016/j.biortech.2011.11.110

Cruz-Olivares J, Pérez-Alonso C, Barrera-Díaz C, Ureña-Nuñez F, Chaparro-Mercado M, Bilyeu B (2013) Modeling of lead (II) biosorption by residue of allspice in a fixed-bed column. *Chemical Engineering Journal* 228:21-27, DOI: 10.1016/j.cej.2013.04.101

Daffalla SB, Mukhtar H, Shaharun MS, Hassaballa AA (2022) Fixed-bed adsorption of phenol onto microporous activated carbon set from rice husk using chemical activation. *Applied Sciences* 12:4354, DOI: 10.3390/app12094354

de Araujo CMB, Ghislandi MG, Rios AG, da Costa GRB, do Nascimento BF, Ferreira AFP, da Motta Sobrinho MA, Rodrigues AE (2022) Wastewater treatment using recyclable agar-graphene oxide biocomposite hydrogel in batch and fixed-bed adsorption column: Bench experiments and modeling for the selective removal of organics. *Colloids and Surfaces A: Physicochemical and Engineering Aspects* 639:128357, DOI: 10.1016/j.colsurfa.2022.128357

El-Kamash AM (2008) Evaluation of zeolite A for the sorptive removal of Cs^{+} and Sr^{2+} ions from aqueous solutions using batch and fixed bed column operations. *Journal of Hazardous Materials* 151:432-445, DOI: 10.1016/j.jhazmat.2007.06.009

Ersoy B, Sariisik A, Dikmen S, Sariisik G (2010) Characterization of acidic pumice and determination of its electrokinetic properties in water. *Powder Technology* 197:129-135, DOI: 10.1016/j.powtec.2009.09.005

Futalan CM, Yang J-H, Phatai P, Chen I-P, Wan M-W (2020) Fixed-bed adsorption of copper from aqueous media using chitosan-coated bentonite, chitosan-coated sand, and chitosan-coated kaolinite. *Environmental Science and Pollution Research* 27:24659-24670, DOI: 10.1007/s11356-019-06083-0

Gatea MA, Jumaah GF, Al Anbari RH, Alsalhy QF (2023) Review on decontamination manners of radioactive liquids. *Water, Air, & Soil Pollution* 234:652, DOI: 10.1007/s11270-023-06678-x

Gatea MA, Jumaah GF, Alsalhy QF (2024) Decontaminating liquid-containing Cs-137 by natural Pumice stone. *Journal of Environmental Radioactivity* 272:107342, DOI: 10.1016/j.jenvrad.2023.107342

Gatea MA, Kadhum SJ (2019) Radioactive safety assessment for surface contamination by using SAFRAN tool. *Journal of Madenat Alelem University College* 11:93-102, https://www.iasj.net/iasj/download/9e3cdac2fff98e2e

Geleta WS, Alemayehu E, Lennartz B (2021) Volcanic rock materials for defluoridation of water in fixed-bed column systems. *Molecules* 26:977, DOI: 10.3390/molecules26040977

Hadi M, Samarghandi MR, McKay G (2011) Simplified fixed bed design models for the adsorption of acid dyes on novel pine cone derived activated carbon. *Water, Air, & Soil Pollution* 218:197-212, DOI: 10.1007/s11270-010-0635-2

Han R, Zou L, Zhao X, Xu Y, Xu F, Li Y, Wang Y (2009) Characterization and properties of iron oxide-coated zeolite as adsorbent for removal of copper (II) from solution in fixed bed column. *Chemical Engineering Journal* 149:123-131, DOI: 10.1016/j.cej.2008.10.015

Ismail A, El-Shafey O, Amr M, El-Maghraby M (2014) Pumice characteristics and their utilization on the synthesis of mesoporous minerals and on the removal of heavy metals. *International Scholarly Research Notices*, 2014, DOI: 10.1155/2014/259379

Juan CA, Pérez de la Lastra JM, Plou FJ, Pérez-Lebeña E (2021) The chemistry of reactive oxygen species (ROS) revisited: Outlining their role in biological macromolecules (DNA, lipids and proteins) and induced pathologies. *International Journal of Molecular Sciences* 22:4642, DOI: 10.3390/ijms22094642

Karabayir E, Ozdemir A, Senkal BF, Taskin OS (2019) A radioactively durable melamine-styrene based polymer: Highly efficient removal of 90Sr. *Applied Radiation and Isotopes* 149:96-103, DOI: 10.1016/j.apradiso.2019.04.024

Karabayir E, Taskin OS, Ozdemir A, Senkal BF (2021) Effective removal of 137Cs ions from radioactive wastewater by Melamine-Styrene based Polymer (MSP). *Applied Radiation and Isotopes* 176:109912, DOI: 10.1016/j.apradiso.2021.109912

Li H, Chen X, Shen D, Wu F, Pleixats R, Pan J (2021) Functionalized silica nanoparticles: Classification, synthetic approaches and recent advances in adsorption applications. *Nanoscale* 13:15998-16016, DOI: 10.1039/D1NR04048K

Metwally SS, Ahmed IM, Rizk HE (2017) Modification of hydroxyapatite for removal of cesium and strontium ions from aqueous solution. *Journal of Alloys and Compounds* 709:438-444, DOI: 10.1016/j.jallcom.2017.03.156

Nasar A, Mashkoor F (2019) Application of polyaniline-based adsorbents for dye removal from water and wastewater — a review. *Environmental Science and Pollution Research* 26:5333-5356, DOI: 10.1007/s11356-018-3990-y

Nuccetelli C, Rusconi R, Forte M (2012) Radioactivity in drinking

water: Regulations, monitoring results and radiation protection issues. *Annali Dell'istituto Superiore di Sanità* 48:362-373, DOI: 10.4415/ANN_12_04_04

Obrador E, Salvador-Palmer R, Villaescusa JI, Gallego E, Pellicer B, Estrela JM, Montoro A (2022) Nuclear and radiological emergencies: Biological effects, countermeasures and biodosimetry. *Antioxidants* 11:1098, DOI: 10.3390/antiox11061098

Osmanlioglu AE (2018) Decontamination of radioactive wastewater by two-staged chemical precipitation. *Nuclear Engineering and Technology* 50:886-889, DOI: 10.1016/j.net.2018.04.009

Park CW, Kim BH, Yang H-M, Seo B-K, Moon J-K, Lee K-W (2017) Removal of cesium ions from clays by cationic surfactant intercalation. *Chemosphere* 168:1068-1074, DOI: 10.1016/j.chemosphere.2016.10.102

Patel H (2020) Batch and continuous fixed bed adsorption of heavy metals removal using activated charcoal from neem (Azadirachta indica) leaf powder. *Scientific Reports* 10:16895, DOI: 10.1038/s41598-020-72583-6

Patel P, Gupta S, Mondal P (2022) Modeling of continuous adsorption of greywater pollutants onto sawdust activated carbon bed integrated with sand column. *Journal of Environmental Chemical Engineering* 10:107155, DOI: 10.1016/j.jece.2022.107155

Pereira W, do Carmo A, Kelecom A, Kuster A, Ravallet P, Novaes F, Rodrigues J, Lima B, Gonçalves R, Santos R (2019) Radionuclides gamma emitters in muscle tissue in fish and your contribution for dose biota at Funil Dam, Resende, RJ, Brazil. Proceedings of the INAC 2019: International nuclear atlantic conference. Nuclear new horizons: Fueling our future, 2019, https://www.researchgate.net/profile/Wagner-Pereira-6/publication/336440997

Qian W, Song Q, Ding H, Xie W (2019) Computational simulations of the mass transfer zone in GS adsorption column packed with Fe^{3+} type ion exchanger. *Chemosphere* 215:507-514, DOI: 10.1016/j.chemosphere.2018.10.054

Rajib M, Oguchi CT (2017) Adsorption of ^{133}Cs and ^{87}Sr on pumice tuff: A comparative study between powder and intact solid phase. *Acta Geochimica* 36:224-231, DOI: 10.1007/s11631-016-0133-3

Ratnawati R, Enjarlis E, Husnil YA, Christwardana M, Slamet S (2020) Degradation of phenol in pharmaceutical wastewater using TiO_2/pumice and O_3/active carbon. *Bulletin of Chemical Reaction Engineering & Catalysis* 15:146-154, DOI: 10.9767/bcrec.15.1.4432.146-154

Raut M-S, Mei H, Mei D-M, Bhattarai S, Wei W-Z, Panth R, Acharya P, Wang G-J (2020) Characterization of high-purity germanium (Ge) crystals for developing novel Ge detectors. *Journal of Instrumentation* 15:T10010, DOI: 10.1088/1748-0221/15/10/T10010

Ravindra A, Kulkarni D, Sharma R, Sathian V, Chaudhury P, Aswal D (2023) National audit for traceable 131I activity measurements with radionuclide calibrators among nuclear medicine Centers in India. *MAPAN*, 1-13, DOI: 10.1007/s12647-023-00645-x

Riazi M, Keshtkar AR, Moosavian MA (2016) Biosorption of Th (IV) in a fixed-bed column by Ca-pretreated Cystoseira indica. *Journal of Environmental Chemical Engineering* 4:1890-1898, DOI: 10.1016/j.jece.2016.03.017

Soto ML, Moure A, Domínguez H, Parajó JC (2017) Batch and fixed bed column studies on phenolic adsorption from wine vinasses by polymeric resins. *Journal of Food Engineering* 209:52-60, DOI: 10.1016/j.jfoodeng.2017.04.008

Tokar E, Tutov M, Bratskaya S, Egorin A (2022) Removal of Cs-137 radionuclide by resorcinol–formaldehyde ion-exchange resins from solutions simulating real liquid radioactive waste. *Molecules* 27:8937, DOI: 10.3390/molecules27248937

Tomkins KM (2014) Uncertainty in streamflow rating curves: Methods, controls and consequences. *Hydrological Processes* 28:464-481, DOI: 10.1002/hyp.9567

Tuaimah SK, Al-Nasri SK, Al-Rahmani AA, Abbas T (2020) Using dates leaves midribs to prepare hierarchical structures incorporating porous carbon and zeolite a composites for cesium137Cs ion exchange. *Baghdad Science Journal* 17:0818, DOI: 10.21123/bsj.2020.17.3.0818

Xu C, Wang J, Chen J (2012) Solvent extraction of strontium and cesium: A review of recent progress. *Solvent Extraction and Ion Exchange* 30:623-650, DOI: 10.1080/07366299.2012.700579

Zhang Y, Xiong L, Xiu Y, Huang K (2019) Defluoridation in fixed bed column filled with Zr (IV)-loaded garlic peel. *Microchemical Journal* 145:476-485, DOI: 10.1016/j.microc.2018.11.007

Zhou H, Zhu X, Chen B (2020) Magnetic biochar supported α-MnO_2 nanorod for adsorption enhanced degradation of 4-chlorophenol via activation of peroxydisulfate. *Science of The Total Environment* 724:138278, DOI: 10.1016/j.scitotenv.2020.138278